Can. J. Remote Sensing, Vol. 28, No. 3, pp. 385–393, 2002

Wave height and wind direction from the HF coastal ocean surface radar

Malcolm L. Heron and Arnstein Prytz

Abstract. The biggest difficulty in extracting wind direction from high-frequency (HF) backscatter ground-wave radar data is in not knowing the fundamental shape of the directional spreading function at the Bragg wavelength for the sea-surface gravity waves. In this paper we present data from a deployment of the HF coastal ocean surface radar (COSRAD) which samples the same patch of water from a range of different angles, allowing us to determine the shape of the spectral spreading function for the Bragg resonant gravity waves. The resulting evaluation of wind direction compares favourably with wind-vane measurements in the vicinity. A routine method for extracting root mean square (rms) wave heights from HF backscatter ground-wave radar spectra has been developed based on the theoretical work of D.E. Barrick. This method is reviewed in the paper and a "best practice" procedure is described for routine production of rms wave heights. Results are shown for a recent deployment of the COSRAD HF radar near Cairns in the Great Barrier Reef Region of northeast Australia. The observed rms wave heights agree reasonably well with those given by the JONSWAP model over the same range of wind speeds. A method for obtaining a measure of the spreading of the directional wave spectrum has been developed. Over the period of observation, the wind speeds varied between 2 and 11 m/s, and the S values for the M.S. Longuet-Higgins et al. spreading function were in the range 1.94 ± 0.62. These S values are less than those given by the JONSWAP model, especially at low wind speeds. A sensitivity study was carried out on the spread of wind directions which would arise from this variability in the wave directional spreading function. For single measurements, the error in wind direction is ±25°, but with spectral averaging over time and space the HF radar errors in wind directions are reduced to about ±10°.

Résumé. La plus grande difficulté dans l'extraction de la vitesse du vent à partir des données de rétrodiffusion radar HF de surface provient du fait que l'on ne connaît pas la forme de base de la fonction d'étalement directionnel à la longueur d'onde de Bragg pour les ondes de gravité à la surface de la mer. Dans cet article, nous présentons des données acquises par le capteur HF COSRAD (HF coastal ocean surface radar) qui échantillonne la même surface d'eau à partir de différents angles, permettant ainsi de déterminer la forme de la fonction d'étalement spectral pour les ondes de gravité de la résonance de Bragg. L'évaluation résultante de la direction du vent se compare avantageusement aux mesures réalisées au moyen de girouettes dans le secteur. Une méthode usuelle pour l'extraction des valeurs rms des hauteurs de vague à partir des spectres de rétrodiffusion radar HF de surface a été développée basée sur les travaux théoriques de D.E. Barrick. Dans cet article, on décrit la méthode ainsi qu'une procédure de « meilleure pratique » pour la production routinière de hauteurs de vague rms. On y présente les résultats d'une campagne de mesures récente utilisant le radar HF COSRAD, près de Cairns dans la région de la Grande barrière de corail du nord-est de l'Australie. Les valeurs observées de hauteur de vague rms sont raisonnablement en accord avec les valeurs fournies par le modèle JONSWAP par rapport à la même gamme de vitesses de vent. Une méthode pour obtenir une mesure de l'étalement du spectre directionnel de la vague a été développée. Durant la période d'observation, les vitesses de vent variaient entre 2 et 11 m/s et les valeurs de S pour la fonction d'étalement de M.S. Longuet-Higgins et al. se situaient dans la fourchette 1,94 ± 0,62. Ces valeurs de S sont inférieures à celles du modèle JONSWAP, spécialement pour les basses vitesses de vent. Une étude de sensibilité a été réalisée sur l'étalement des directions de vent qui proviendrait de la variabilité dans la fonction d'étalement directionnel de la vague. Pour des mesures uniques, l'erreur dans la direction du vent est de ±25°, mais en appliquant un moyennage spectral par rapport au temps et à l'espace, les erreurs radar HF dans les directions de vent sont réduites à environ ±10°.
[Traduit par la Rédaction]

Introduction

High-frequency (HF) ocean surface radars have been widely used to measure surface currents in coastal waters, and this has become a routine application of the technology. In a recent paper, Graber et al. (1997) report on a comprehensive validation study between surface currents measured by an HF radar and currents measured by traditional techniques. This work provides confidence in the surface-current product emerging from the HF radar technique.

HF radars can also be used to evaluate some parameters of the directional wave spectrum of sea-surface gravity waves. Much effort has gone into the extraction of full directional wave spectra from dual-station HF radar data (Wyatt and Holden, 1994). This full analysis needs to have good signal to noise

Received 1 May 2001. Accepted 21 February 2002.

M.L. Heron[1] and A. Prytz. School of Mathematical and Physical Sciences, James Cook University, Townsville, Queensland, Australia 4811.

[1]Corresponding author (e-mail: mal.heron@jcu.edu.au).

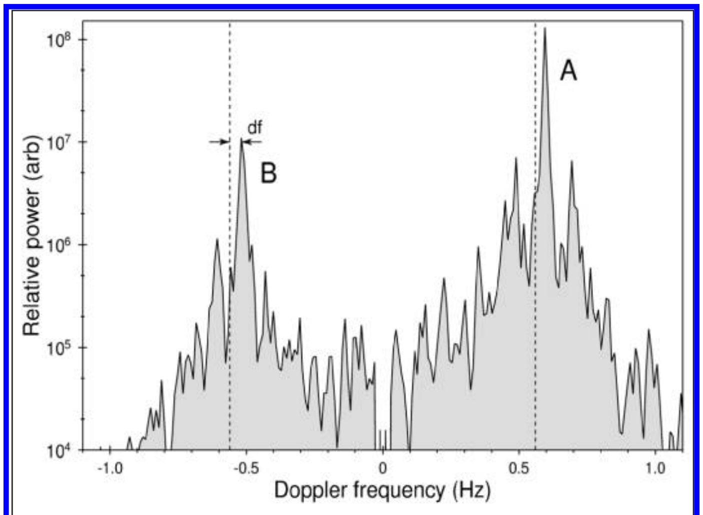

Figure 1. A typical Doppler shift spectrum from the COSRAD HF (30 MHz) radar, showing Bragg peaks A and B and the continuum of second-order energy surrounding them.

ratios in the radar data and requires a reasonably intensive analysis effort. Graber and Heron (1997) have shown that an original theoretical analysis by Barrick (1977) can be applied to produce real-time values of significant wave height from a single HF radar station and, of course, a commensurate improvement in data quality if two overlapping radars are used.

One of the intrinsic niceties of Wyatt's full wave directional analysis (Wyatt and Holden, 1994) is that the spreading parameter is evaluated from the data. This is in contrast with most other remote sensing techniques for wind direction, where the shape of the spreading function has to be assumed. This includes most deployments of HF ocean radar systems to measure wind directions, for example, Georges et al. (1993) and Fernandez et al. (1997).

This paper has two main innovations. One is to remove the directional ambiguity using the data from one radar station. The other is to use the HF radar data to evaluate the spreading parameter for the sea-surface waves over the area of ocean being observed. This is an important study because it indicates what parameter should be used for the spreading function if we were restricted to using an assumed value.

Methodology and study site

When a vertically polarised HF wave propagates in groundwave mode over the ocean, some of the energy scatters from the rough conducting surface. Using a coherent, narrow-beam radar, we can log a time series for each range step. The coastal ocean surface radar (COSRAD) used in this study operates at 30 MHz and dwells for 102.4 s in each azimuthal direction. A typical Doppler shift spectrum of the received echoes is shown in **Figure 1**. It has two dominant first-order spectral lines corresponding to a Bragg scatter from resonant sea-surface waves propagating away from the radar (marked B in **Figure 1**) and those propagating towards the radar (marked A in

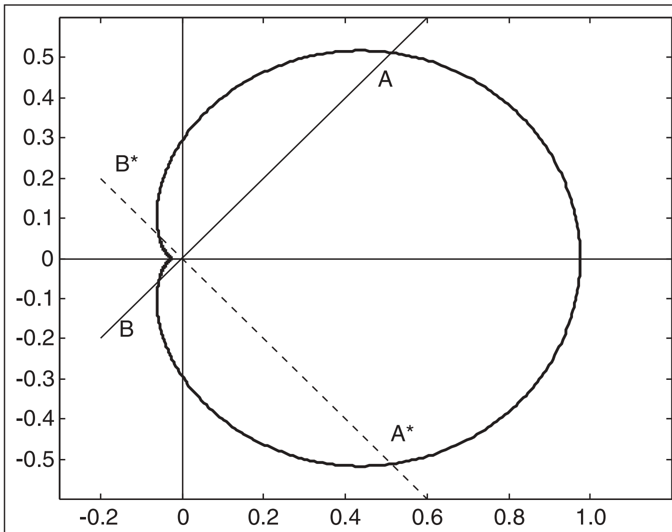

Figure 2. The spreading function assumed for the wave directional spectrum with an S value of 2. The line from the origin to A illustrates a radar beam position, with A^* indicating the ambiguity point.

Figure 1). The energy in these two spectral lines relates to the relative amplitude of the Bragg waves on the sea surface. In **Figure 1**, for example, it is clear that the Bragg wave propagating towards the radar (peak A) has greater amplitude than the Bragg wave propagating away from the radar (peak B). We interpret this to mean that the wind vector has a component towards the radar at the pixel being observed. These are high-energy first-order spectral peaks which are some 20–60 db above the base noise level in the spectrum. The ratio of the energy in spectral lines A and B can be used to determine the direction of the wind and, under some circumstances, the spreading function for the wind-generated waves.

Longuet-Higgins et al. (1963) suggested the following form for the spreading function G:

$$G(\theta) = A\cos^{2S}\left(\frac{\theta - \theta_w}{2}\right) \tag{1}$$

where A is a normalizing factor required to make $\int_0^{2\pi} G(\theta)d\theta = 1$ for each value of the spreading parameter S; and θ_w is the wind direction, assumed to be the direction of the highest wind waves. It can be shown that

$$A = \frac{2^{2S-1}\Gamma^2(S+1)}{\pi\Gamma(2S+1)}, \tag{2}$$

where Γ is the factorial gamma function. The directional spreading function G is shown in **Figure 2** where, for illustration, the antenna beam points from B to A and the wind is directed along the x axis. The ratio of the first-order lines would then correspond to the ratio of OA to OB, where O is the origin. For a given S value there are two possible beam directions, namely B to A and B^* to A^*. The duplicity is

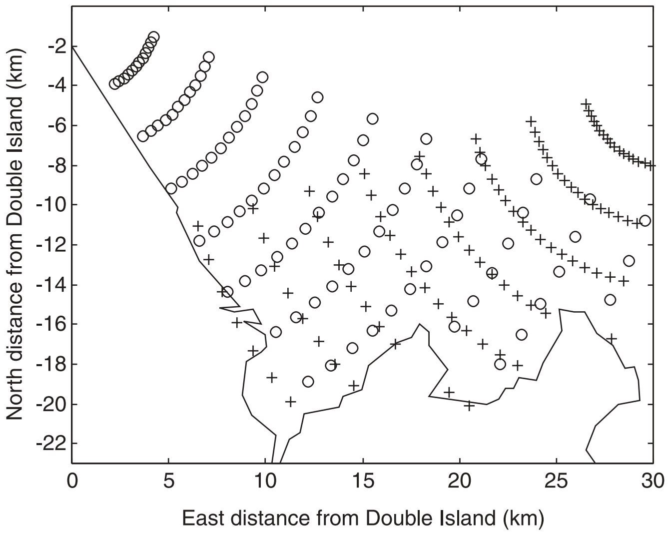

Figure 3. Study area showing the locations of the observation points on the sea surface. The coastline is shown as a solid line. +, sites observed from the Green Island radar station; ○, sites observed from the Double Island station.

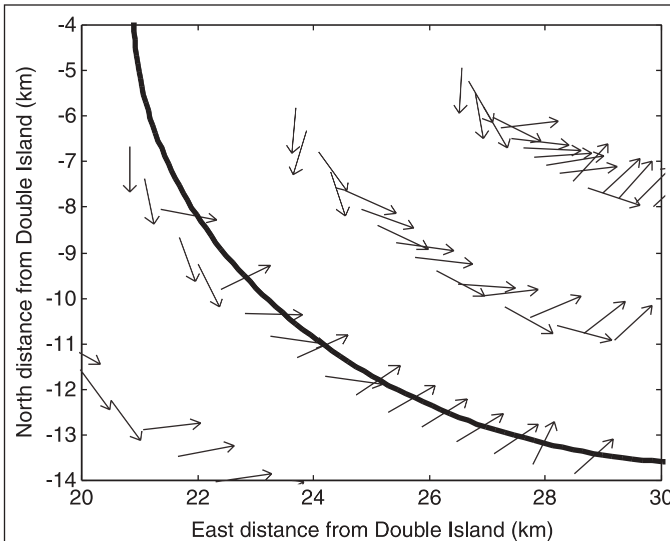

Figure 5. Observed sites within 10 km of Green Island (solid line), showing the positive-sign ambiguity in wind direction. The arrows are of equal length and their direction indicates a possible interpretation for wind direction.

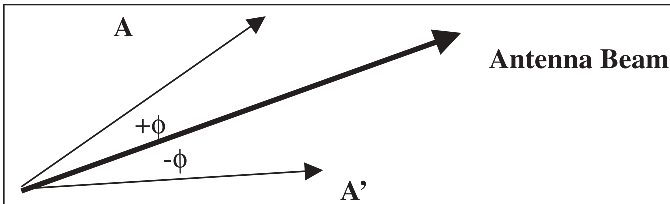

Figure 4. When the antenna beam direction is fixed and the ratio of first-order energies, R, is measured, the wind direction is determined to be in the direction A or A' with the ambiguity shown.

inherent in the method and always appears as an ambiguity in the wind direction with respect to the direction of the antenna beam.

In this work, the ambiguity is resolved by a spatial analysis, using the ability of the radar system to steer the beam to different azimuth angles and sample the ocean over a short period of time (about 30 min).

Mapping is carried out by electronically steering the beam and time-gating radar pulses to produce range resolution. The study site was in northeastern Australia on the Great Barrier Reef, in Trinity Bay near the city of Cairns. The radar stations were located at Green Island (latitude 16°45′41.0″S, longitude 145°58′12.4″E) and Double Island (latitude 16°43′43.9″S, longitude 145°40′48.0″E). Our local grid reference system sets the origin at the Double Island station, and maps are plotted in kilometres east and kilometres north from that origin. Green Island is at grid coordinates (32.24 km, –3.61 km). The radar coverage is shown in **Figure 3**, where the solid line represents the coast.

Wind direction mapping

When the radar beam is set in a particular direction and the ratio $R = A/B$ is measured, the ambiguity appears as an uncertainty of $\pm\phi$ in the wind direction, as shown in **Figure 4**, where ϕ, the wind direction measured with respect to the antenna beam direction, is determined from (Heron and Rose, 1986)

$$\phi = \left|2\arctan(R^{1/2s})\right| \tag{3}$$

The methodology used to remove the ambiguity is to evaluate consistency in the wind direction over the range of azimuths of the antenna beam. In this section we adopt a value of $S = 2$ for the spreading parameter to illustrate the procedure. In a later section (i.e., Wave direction model) we repeat these wind direction calculations with S values between 1 and 6 to find a best-fitting S value. It is a simple matter to produce the wind direction maps with the optimum S value.

In practice, the beam is steered by altering the signal phase to the elements of a linear antenna array. Considerations of beam width and impedance matching limit the amount of steering to ±30° from the bore-sight direction. For pixels within 10 km of the radar station, the area sampled is about 50 km^2 and we assume that the wind direction is approximately constant over that area. **Figure 5** shows an arc of radius 10 km centred on Green Island for one 0.5 h sweep through the beam positions. It also shows the wind directions obtained by taking the negative ambiguity option; **Figure 6** shows the same data set but obtained by taking the positive ambiguity option. If the wind direction is indeed constant over the area, then the wrong choice will produce a change in the extracted wind direction of

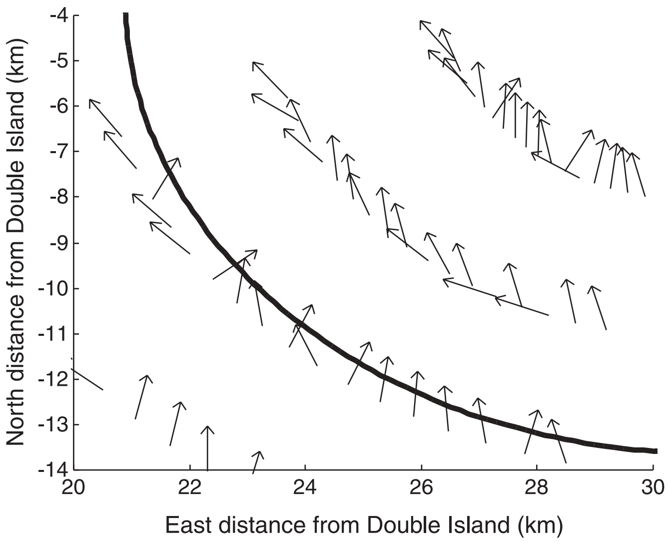

Figure 6. Observed sites within 10 km of Green Island (solid line), showing the negative-sign ambiguity in wind direction. The arrows are of equal length and their direction indicates a possible interpretation for wind direction.

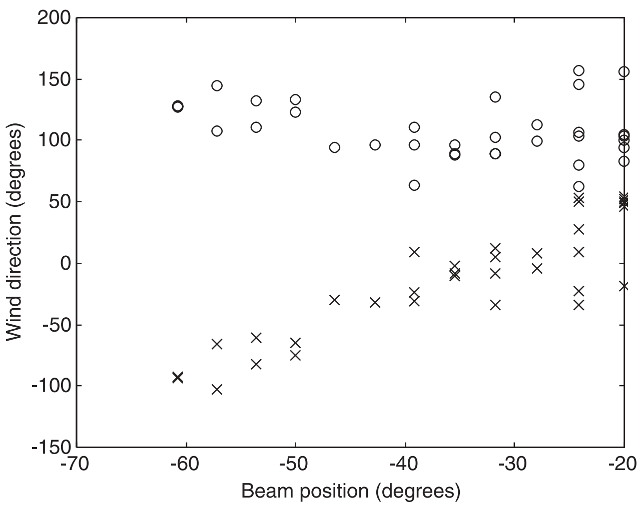

Figure 7. Resolution of the positive–negative ambiguity. The extracted wind direction is plotted against the direction of the antenna beam as it sweeps through an arc of about 60°. ○, results based on the negative ambiguity condition; +, results based on the positive ambiguity condition.

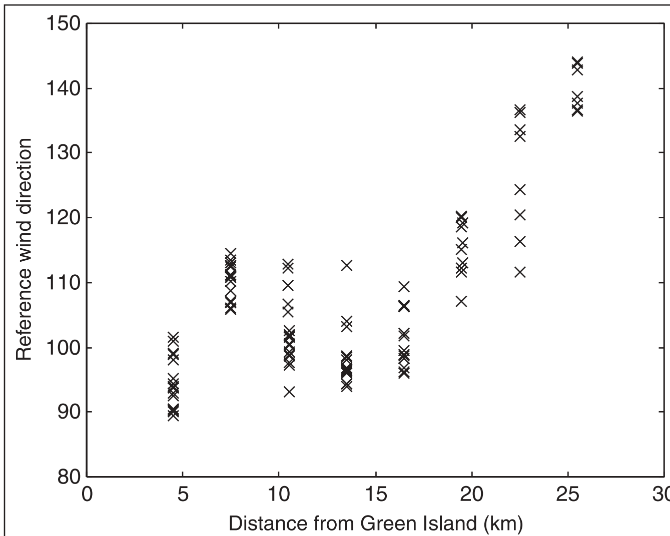

Figure 8. The reference wind direction is allowed to vary slowly as we step away from the Green Island radar station.

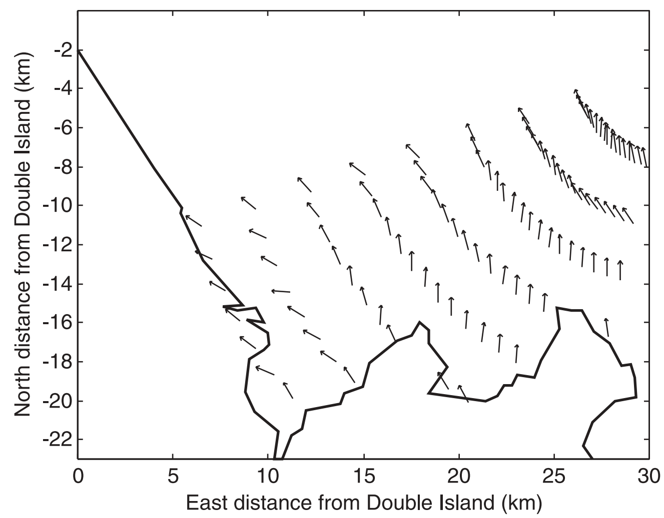

Figure 9. Wind directions observed from the Green Island radar station.

$2\Delta\theta$ for every shift $\Delta\theta$ of the antenna beam, whereas the correct choice will produce no change. This is illustrated in **Figures 5** and **6**, which plot the derived wind directions for the positive (**Figure 5**) and negative (**Figure 6**) ambiguities. The analysis algorithm has to determine which of these produces the more stable wind direction as the radar antenna beam is moved through the arc shown.

Theoretically, the correct ambiguity condition has a zero slope on the best-fitting straight line in **Figure 7**. Based on experience with noisy data, we have found that a more reliable algorithm is to adopt the ambiguity condition which has the smaller mean square deviation from the mean wind speed as the beam position changes.

The ambiguity condition adopted in this way, for points near to the radar station, may not be correct across the whole area. We sort the observation sites into order of increasing distance from the radar station and work progressively outwards using a reference wind direction to solve the ambiguity at each site. The reference direction is a weighted average of wind directions analysed up to that point but weighted towards the most recent. At each site on the grid map, the ambiguity is solved by taking the option closest to the reference direction. This allows us to accept changes in the wind direction as we move across the map. **Figure 8** shows how the reference wind direction changed across the mapped area from the Green

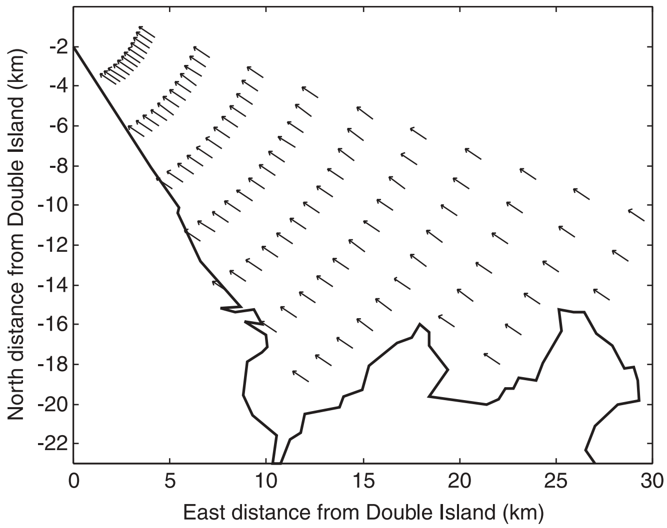

Figure 10. Wind directions observed from the Double Island radar station.

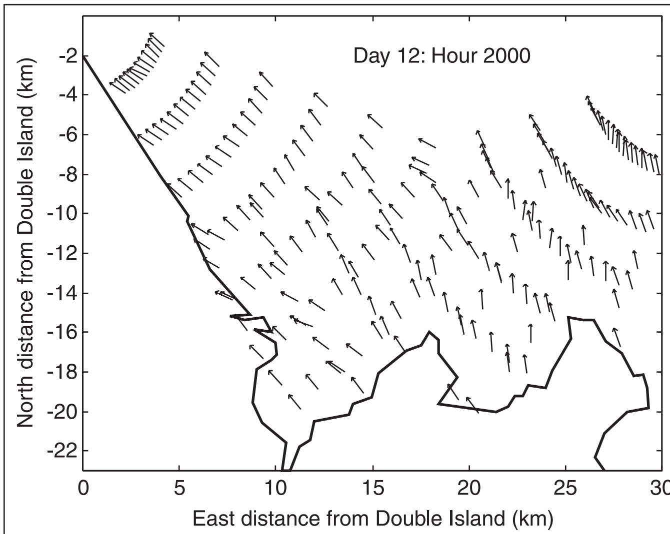

Figure 11. Composite wind direction map for the Trinity Bay area.

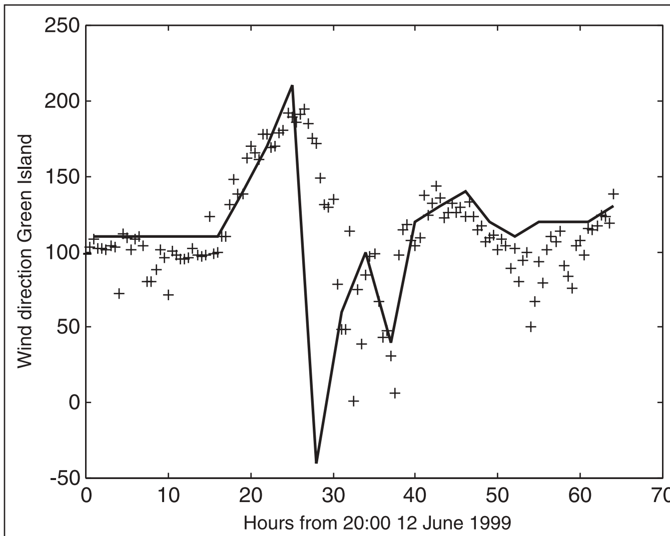

Figure 12. Time series of wind directions for radar sea-surface sites within 5 km of Green Island (+) and 3 h wind direction data from the anemometer at Green Island (solid line).

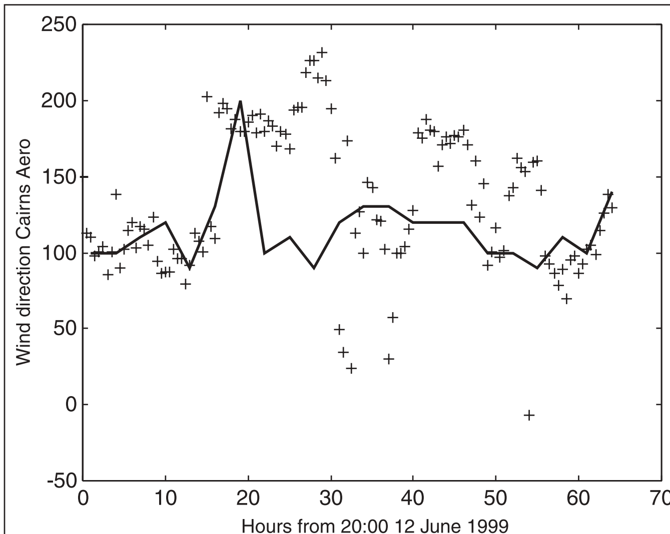

Figure 13. Time series of wind directions for radar sea-surface sites within 5 km of Cairns Airport (+) and 3 h wind direction data from the anemometer at the Cairns Airport (solid line).

Island radar station. The resulting map of wind directions is shown in **Figure 9**.

The analysis is repeated for the Double Island data to produce an independent map of wind directions over the same time period (**Figure 10**). The final step is to combine the data from the two stations and spatially smooth the data by averaging each data point with its four nearest neighbours. The final map of wind directions is shown in **Figure 11**.

Comparison with anemometers

Anemometer data were available at 3 h intervals from stations at Green Island and Cairns Airport (grid position (8.2 km, –17.1 km) in **Figure 3**). To make a comparison, we averaged the radar wind directions from all observation sites within 5 km of the Green Island anemometer and, separately, all sites within 5 km of the Cairns Airport anemometer. The time series of three-hourly directions from the Green Island anemometer are shown as the solid line in **Figure 12**, and the plotted points are the 0.5 h radar-determined values. The corresponding data for the Cairns Airport are shown in **Figure 13**.

The Green Island radar and anemometer data show reasonable agreement, but with an offset of about 15° when the wind is towards the north (90–100° in **Figure 12**). The wind speed at Green Island was above 2 m/s around 28–36 h when a major change in direction occurred.

The radar observations within 5 km of Cairns Airport show better agreement with the observations from the Green Island

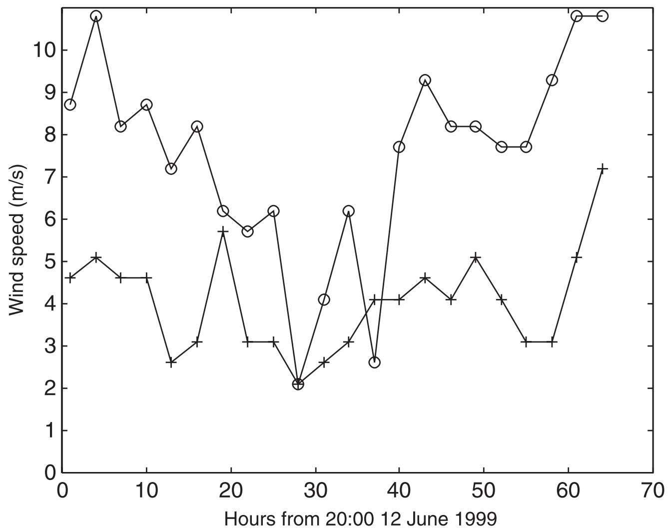

Figure 14. Wind speeds recorded by the anemometers at Green Island (○) and Cairns Airport (+).

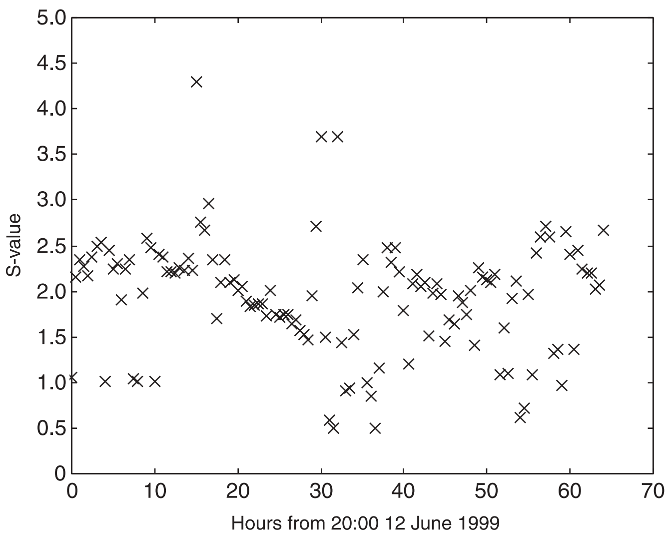

Figure 15. Time series of S values for the directional wave model.

anemometer than with those from the Cairns Airport anemometer. Factors that may be affecting this comparison include the topographic effects of hills close to the Cairns Airport and the contrast in friction between land and sea.

Wind speeds for the Green Island and Cairns Airport anemometer stations are shown in **Figure 14**. Around 25–35 h from the reference time the wind speed at Green Island fluctuates about low values. This corresponds to the period of significant changes in wind direction in **Figure 12**. The analysis for the wind direction from the HF radar data does not perform well when the sea is confused by a mixture of growing and decaying waves. The assumed one-parameter unimodal directional wave spreading function may not be a good model in transient conditions. **Figure 12** indicates that the radar-derived wind directions data are responding to changes within the 3 h interval between the anemometer-derived wind directions.

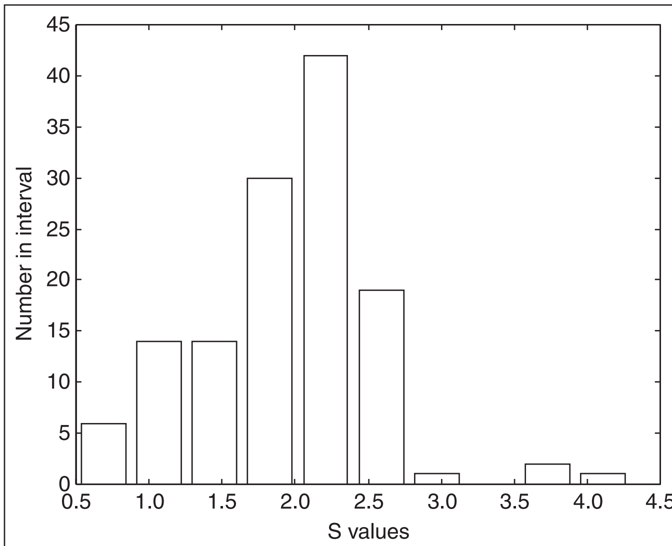

Figure 16. Histogram of S values for the directional wave model.

Wave direction model

The wind direction maps in the preceding section are of limited local interest but illustrate the technique using the spreading parameter value $S = 2$. The values of S under different wind speeds are more global and are of interest in most analysis methods to determine oceanic wind directions from radar backscatter echoes. To estimate the best S value, we repeated the calculations for wind direction, ϕ, at each point with values of S between 1 and 6 and found the mean and standard deviation of wind direction. If the inherent fluctuations in wind direction are less than the errors caused by choosing the wrong value of S, then we would expect to find a minimum in the standard deviation of the wind direction as S is varied. Indeed, we found consistent minima in most cases and could extract the best estimate of S from each 0.5 h record. If there was not a clear minimum, then we extended the range of S values to search for a minimum. **Figure 15** shows a time series of the average S value determined each 0.5 h over the radar-mapped area. The value of S is not very sensitive to the changes in conditions over the 64 h of this campaign. If we assume that the S values are drawn from a statistically stationary population, then the mean is 1.94 and the standard deviation is 0.62. In fact, the S values are not quite stationary and are somewhat more scattered during the lull in wind speeds when the wind direction was rotating. The histogram of S values is shown in **Figure 16**. Overall, the distribution of S values is skewed, with a median of 2.05 and range of 0.5–4.4.

For comparison, the values of S from the JONSWAP data set can be obtained from the model given by Hasselmann et al. (1980):

$$S = S_m \left(\frac{f}{f_m} \right)^{\mu} \qquad f > f_m \tag{4}$$

where

$$S_m = 9.77 \pm 0.43, \tag{5}$$

and

$$\mu = -(2.33 \pm 0.06) - (1.45 \pm 0.45)\left(\frac{U}{c_m} - 1.17\right) \tag{6}$$

and the subscript m refers to the peak in the wave spectrum. For a fully developed spectrum, Pierson and Moskowitz (1964) have

$$f_m = \frac{0.14g}{U_{19.5}}, \tag{7}$$

and $c_m = g/2\pi f_m$.

For wind speeds in the range 2.45–11.00 m/s and wave frequency 0.56 Hz, the JONSWAP S values are in the range 9.77–0.55. Heron (1987) also reported S values that were consistently less than those from the JONSWAP model.

It is useful to know how sensitive the wind directions, ϕ, are to errors in the S value used in the analysis. From Equation (3),

$$\Delta\phi = \frac{-R^{(1-2S)/2S}}{(1 + R^{1/S})S^2}\,\Delta S \tag{8}$$

For S = 1.94 and ΔS = –0.62, 0.00, +0.62 (corresponding to the mean and ± one standard deviation), we plotted the graph of $\Delta\phi$ versus ϕ in **Figure 17**. The angular spread is insensitive to S at ϕ = 90°, when the wind is blowing orthogonal to the radar beam. It peaks at around ϕ = 70° and is typically about ±25° across the range.

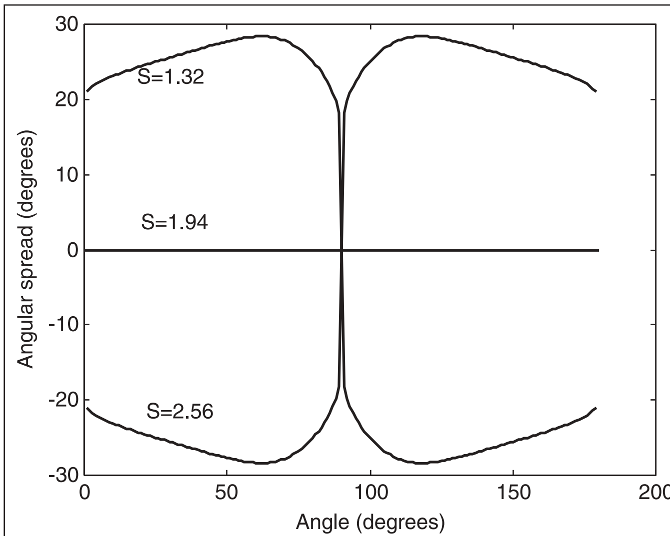

Figure 17. The spread of angles $\Delta\phi$ corresponding to the spread of ± one standard deviation in S, shown with ϕ varying from 0 to 180°.

Wave heights

Estimation of wave heights from Bragg spectra is based on the theoretical work of Barrick (1977) and has been developed and used by many people. These techniques rely on separating the radar echoes into first-order (essentially the narrow Bragg peak) and second-order (wave spectrum) components. It is from the ratio of the second-order energy to the first-order energy that the wave heights (h_s) are obtained, using

$$h_s = \frac{3.11}{k_0}\left(\frac{E_2}{E_1}\right)^{1/2} \tag{9}$$

where k_0 is the wave number of the radar signal, E_1 is the energy in the larger Bragg peak, and E_2 is the weighted second-order energy associated with the larger Bragg peak. Equation (9) is derived from Heron and Heron (1998) by introducing the variable k_0. Calculation of E_2 typically includes all frequencies on one side of the spectrum (positive or negative) but excludes the energy in the (first order) Bragg peak.

To obtain improved signal to noise ratios, one can average a number of spectra in either time or space, with a corresponding loss of temporal or spatial resolution. Because of typically uniform spatial conditions it is often desirable to smooth spatially because the sea responds fairly rapidly to changing wind conditions at wavelengths up to 10 m.

The COSRAD system complicates this process somewhat because the radar spectra obtained from various ranges have different signal to noise ratios. It would not be desirable to simply average these spectra because the higher noise levels in some spectra will overestimate the energy in the second-order part of those spectra, and hence the mean spectrum. The mean spectrum is formed by including only those spectral components, away from the Bragg frequency, up to the point where the spectral energy drops below a predetermined noise level. This noise level is set for each spectrum by selecting the energies at the extremes of the spectrum as being representative of the noise. An alternative technique for establishing the noise level is described by Heron and Heron (1998), who fitted a Rayleigh probability distribution to the noise. For all spectra collected within a given distance of the point being studied, we identify that spectrum with the highest signal to noise ratio. We choose the larger Bragg peak of that spectrum, normalize all other spectra to the height of that Bragg peak, and average the spectra. The number of spectral values that form the average tends to decrease for frequencies farther from the Bragg peak because of our criterion to reject points with low signal to noise ratio. It is from this mean spectrum that the wind-wave height is estimated for COSRAD.

The dimensionless significant wave height $\widetilde{H}_s$ is modelled by Elfouhaily et al. (1997) by

$$\tilde{H}_s = 0.26\left\{\tanh\left[\left(\frac{k'x}{X_0}\right)^{0.4}\right]\right\}^{1.25} \tag{10}$$

where X_0 = 22 000, $k' = g/(U_{10})^2$, and x is the fetch in metres. The root mean square wave heights h_{rms} are then obtained from $h_{rms} = \tilde{H}_s/k'$ for the 3 h wind speeds observed at Green Island (**Figure 14**) and a fetch of 10 km. **Figure 18** compares the modelled values with the radar-derived root mean square wave heights. It can be observed that if we set aside the period when the wind direction was changing, the agreement is quite good, with the radar wave height values being about 5 cm less than those from the model.

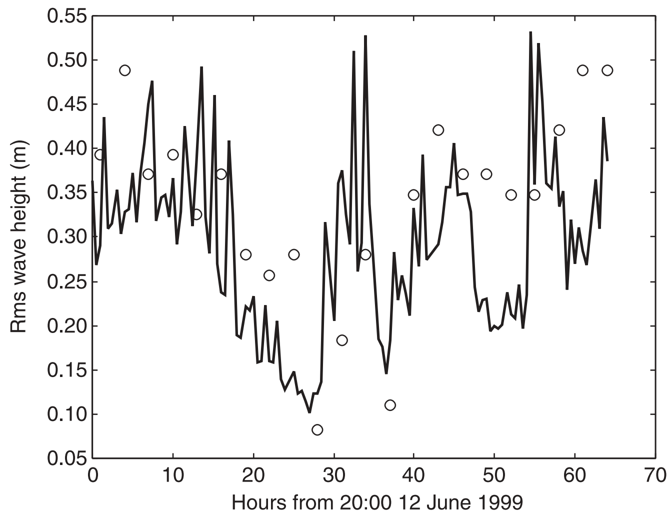

Figure 18. Significant wave heights observed over the area within 5 km of the Green Island radar station. ○, calculated from the model using a fetch of 10 km and the wind speeds observed at Green Island.

Conclusions

High-frequency ocean backscatter radar is a powerful technique for testing the validity of wave spectrum models and relationships between the sea-surface waves and the wind speed and direction. The data discussed in this paper came from a 64 h deployment of a dual-radar system in waters of the Great Barrier Reef lagoon where there is negligible swell.

Wind directions are derived from high signal to noise measurements on the first-order part of the spectrum of echoes, and the HF radar is very reliable at measuring the spreading function of the wind-wave spectrum at the Bragg wavelength. At each 0.5 h interval a map of wind directions was produced, and a mean value of the Longuet-Higgins et al. (1963) spreading parameter S was found. The wind directions averaged over all radar measurements within 5 km of Green Island agreed to about ±10° with 3 h wind directions measured at Green Island. Radar-derived wind directions within 5 km of Cairns Airport showed better agreement with the Green Island anemometer than with the anemometer at the airport, and we suggest that this reflects topographical and thermal effects of the mainland rather than false measurements.

Wave height observations from the HF radar agree reasonably well with wave heights calculated by integrating the elevation spectrum given by Elfouhaily et al. (1997).

Optimized S values were obtained by minimising the standard deviation of wind direction measurements as S is varied in the analysis. This method is appropriate when the mapped area is smaller than the spatial scale of wind variations. The S values obtained from the radar were in the range 0.5–4.4. For the observed range in wind speeds (2–11 m/s), the S values calculated from the JONSWAP model were in the range 0.55–9.77. These results support earlier radar data (Heron, 1987) which indicate that the JONSWAP S values are too large for short wind waves (5 m wavelength), particularly for low wind speeds. Although the spectral spreading function at wavelengths in the range 1–10 m is not of great significance for coastal engineering and many maritime applications, it is important that we improve the model for remote sensing applications. This paper has shown that HF radar is an appropriate instrument to provide that improvement.

Acknowledgments

We are grateful to the managers of Double Island Retreat and Green Island Resort for access and power to the radar observation sites. The research at Green Island was based at the Monkhouse Research Station operated by the Queensland Department of Primary Industries. Funding for the project came within a collaborative venture between the Cairns Port Authority and the Australian Research Council, for which the Chief Investigator was Professor Bob Carter.

References

Barrick, D.E. 1977. Extraction of wave parameters from measured HF sea-echo Doppler spectra. *Radio Science*, Vol. 12, pp. 415–424.

Elfouhaily, T., Chapron, B., Katsaros, K., and Vandemark, D. 1997. A unified directional spectrum for long and short wind-driven waves. *Journal of Geophysical Research*, Vol. 102, pp. 15 781 – 15 796.

Fernandez, D.M., Graber, H.C., Paduan, J.D., and Barrick, D.E. 1997. Mapping ocean wind direction with HF radar. *Oceanography*, Vol. 10, pp. 93–95.

Georges, T.M., Harlan, J.A., Meyer, L.R., and Peer, R.G. 1993. Tracking hurricane Claudette with the U.S. Air Force over-the-horizon radar. *Journal of Atmospheric and Oceanic Technology*, Vol. 10, pp. 441–451.

Graber, H.C., and Heron, M.L. 1997. Wave measurements from HF radar. *Oceanography*, Vol. 10, pp. 90–92.

Graber, H.C., Haus, B.K., Shay, L.K., and Chapman, R.D. 1997. HF radar comparisons with moored estimates of current speed and direction: expected differences and implications. *Journal of Geophysical Research*, Vol. 102, pp. 18 749 – 18 766.

Hasselmann, D.E., Dunkel, M., and Ewing, J.A. 1980. Directional wave spectra observed during JONSWAP 1973. *Journal of Physical Oceanography*, Vol. 10, pp. 1264–1280.

Heron, M.L. 1987. Directional spreading of short wavelength fetch-limited wind waves. *Journal of Physical Oceanography*, Vol. 17, pp. 281–285.

Heron, M.L., and Rose, R.J. 1986. On the application of HF ocean radar to the observation of temporal and spatial changes in wind direction. *IEEE Journal of Oceanic Engineering*, Vol. OE-11, pp. 210–218.

Heron, S.F., and Heron, M.L. 1998. A comparison of algorithms for extracting significant wave height from HF radar ocean backscatter spectra. *Journal of Atmospheric and Oceanic Technology*, Vol. 15, pp. 1157–1163.

Longuet-Higgins, M.S., Cartwright, D.E., and Smith, N.D. 1963. Observations of the directional spectrum of sea waves using the motions of a floating buoy. In *Ocean Wave Spectra, Proceedings of a Conference*. Prentice-Hall Inc., Englewood Cliffs, N.J., pp. 111–136.

Pierson, W.J., and Moskowitz, L. 1964. A proposed spectral form for fully developed wind sea based on the similarity theory of S.A. Kitaigorodskii. *Journal of Geophysical Research*, Vol. 69, pp. 5181–5190.

Wyatt, L.R., and Holden, G.J. 1994. HF radar measurement of multi-modal directional wave spectra. *Global Atmosphere and Ocean System*, Vol. 2, pp. 265–290.